Electronic Supplementary Material (ESI) for Analyst.
This journal is © The Royal Society of Chemistry 2017

Selective phosphatidylcholine double bond fragmentation and localization using Paternó-Büchi reactions and ultraviolet photodissociation

Fabian Wäldchen[a], Simon Becher[a], Patrick Esch[a], Mario Kompauer[a] and Sven Heiles[a]*

[a] *Institute of Inorganic and Analytical Chemistry, Justus Liebig University Giessen, 35392 Giessen, Germany*

Supplementary Information

*Address correspondence to Dr. Sven Heiles:
Institute of Inorganic and Analytical Chemistry
Justus Liebig University Giessen
Heinrich Buff Ring 17
35392 Giessen, Germany
Phone: +49 641 99 34807
e-mail: sven.heiles@anorg.chemie.uni-giessen.de

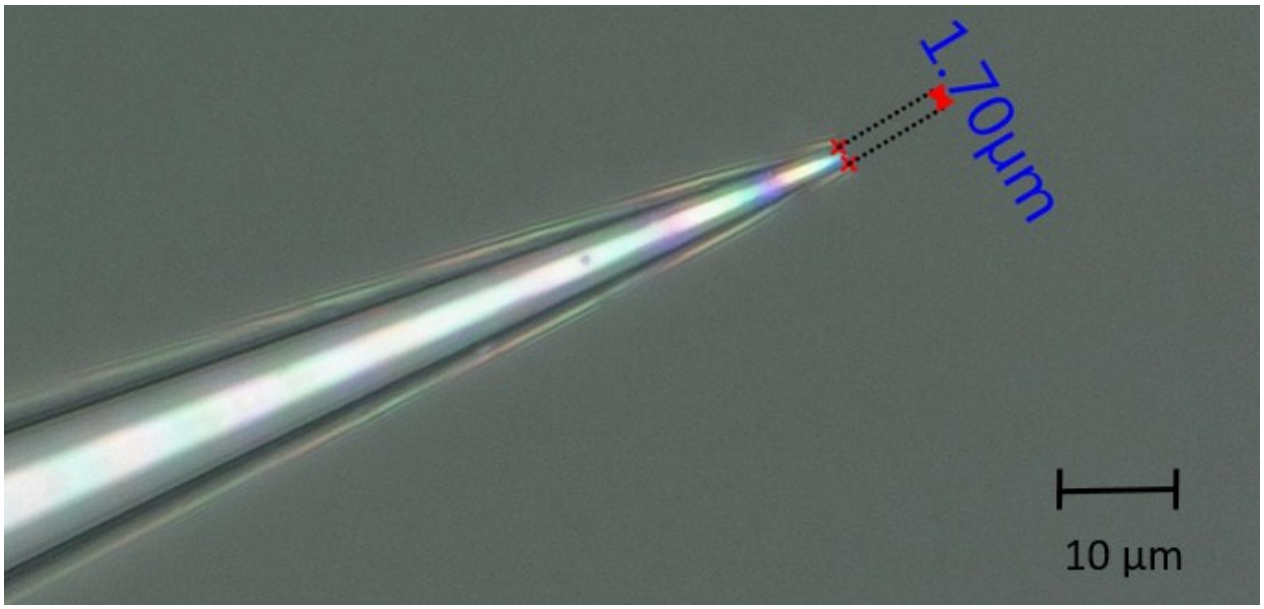

Figure S1. Microscope image of a pulled nanoESI borosilicate emitter for the determination of the inner diameter (i.d.) of the tip. The i.d. of the shown emitter is 1.7 µm (outer dimeter is 1.9 µm). Typical i.d. and o.d. of emitters are between 1.0-2.5 µm.

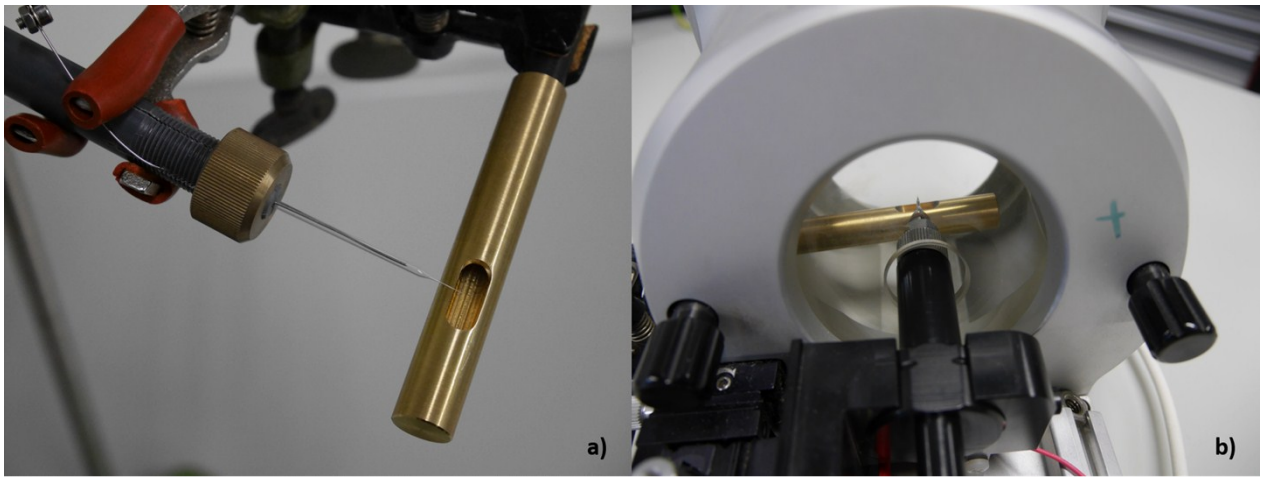

Figure S2. a) Home-built nanoESI source with UV lamp and b) UV lamp integrated in a Thermo Scientific nanoESI source for PB reactions. Sources are shown without protective housing.

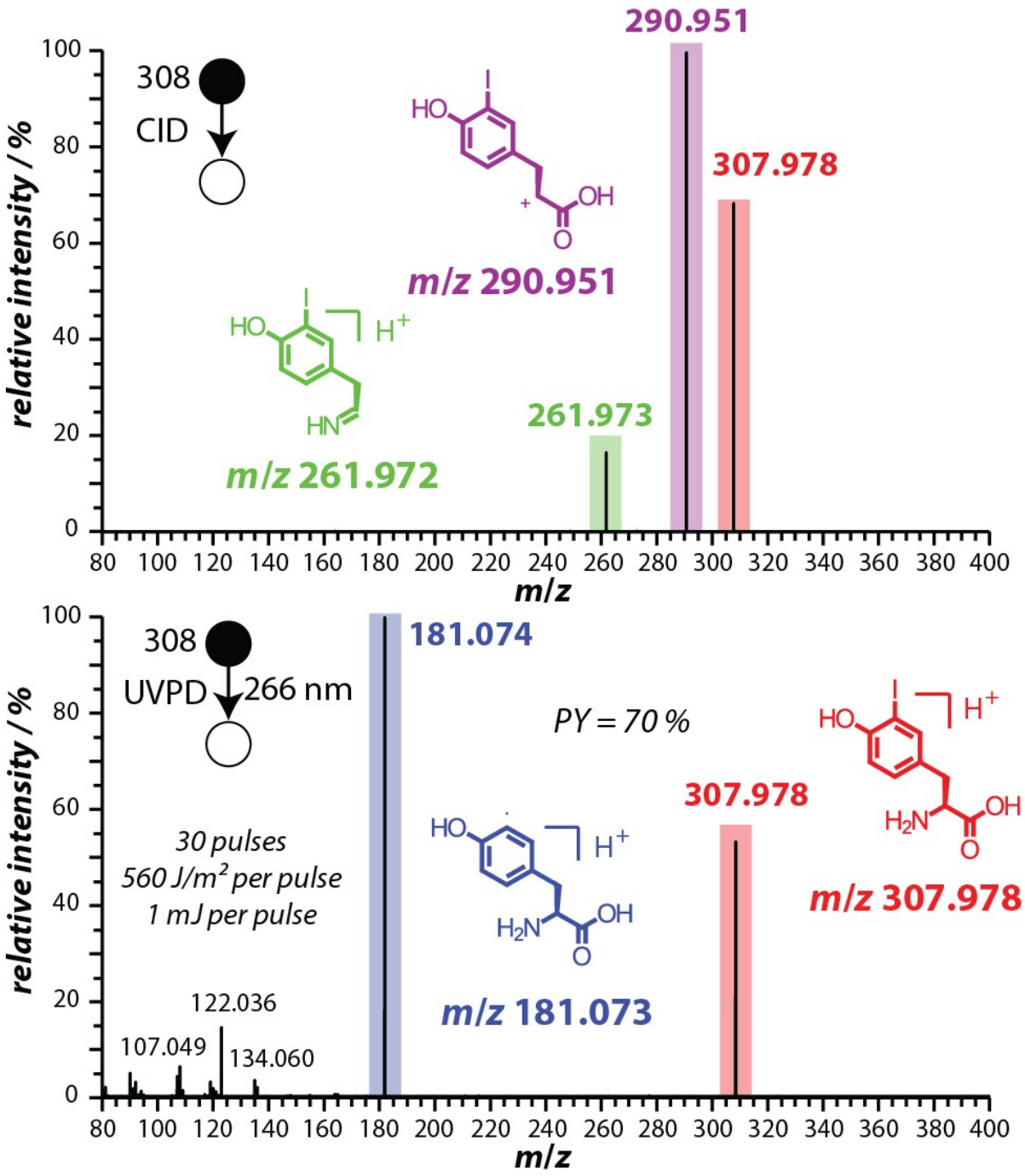

Figure S3. a) Single CID and b) UVPD tandem mass spectra of [3-iodotyrosine+H]$^+$ in positive ion mode. CID was performed with a NCE value of 25 and 30 pulses of a 266 nm Nd:YAG laser with 1 mJ/pulse were used for the UVPD experiments. *PY* and

possible structures of the precursor and fragment ions are included (the ion signals are colour coded accordingly).

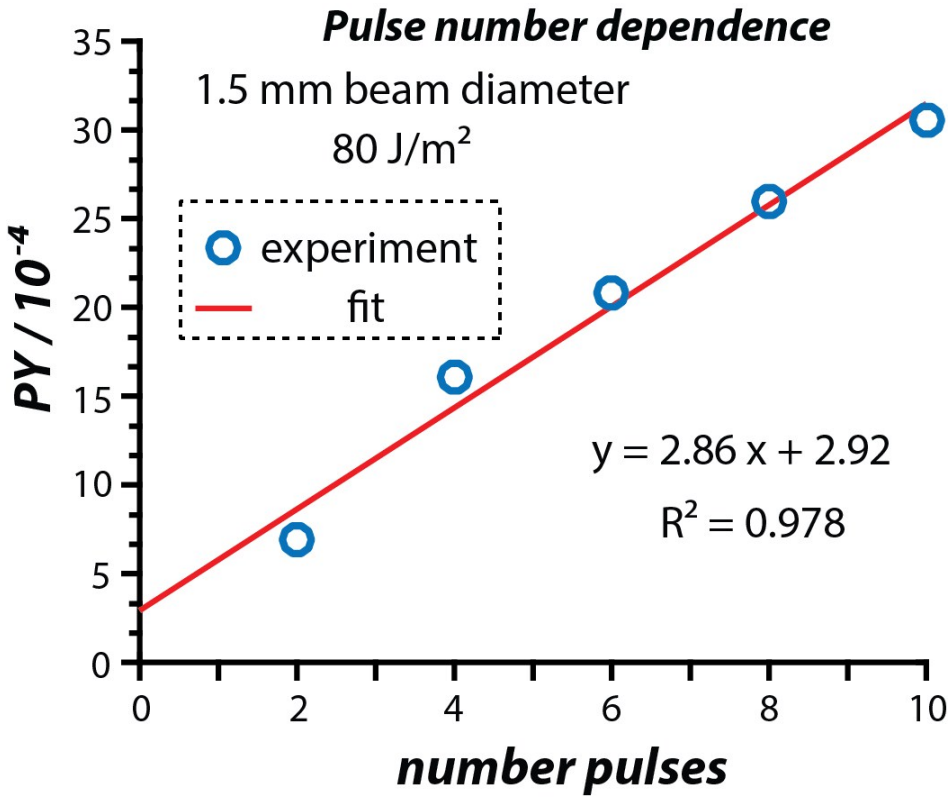

Figure S4. Dependence of *PY* for [3-iodotyrosine+H]$^+$ on the number of laser pulses (266 nm). In order to avoid multiphoton processes or sequential photon absorption, a two laser fluence of 80 J/m^2 was used and the ion at *m/z* 181.073 was the only detected fragment consistent with previous results.[2]

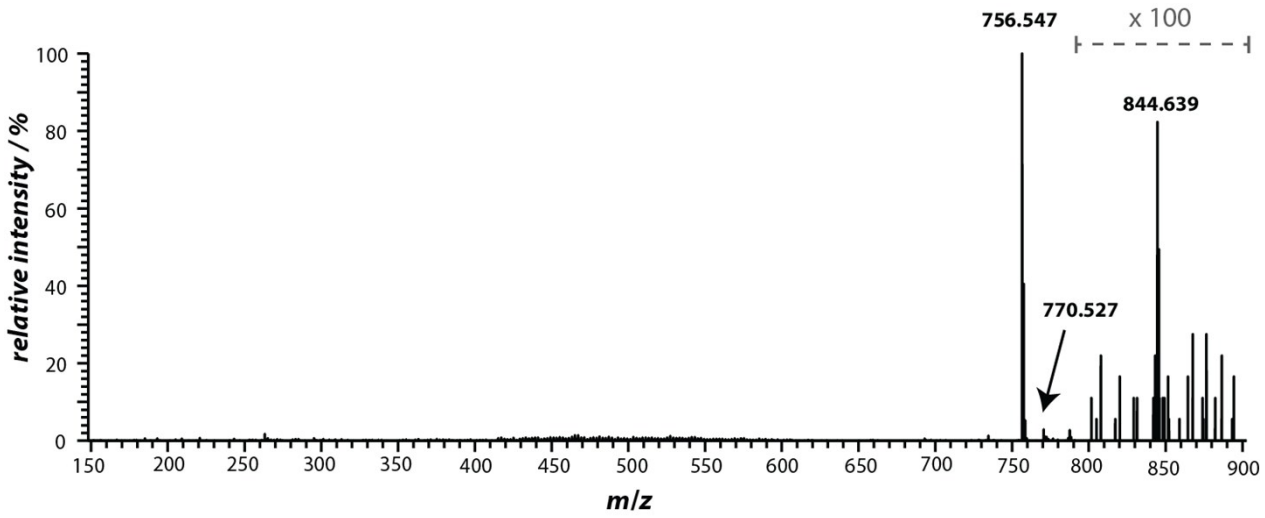

Figure S5. Positive nanoESI mass spectrum of sodiated PC 16:0/16:0 (*m*/*z* 756.547). The region between *m*/*z* 800-900 is magnified by x100. No signal above signal to noise is detectable at *m*/*z* 756.547 + 120.057 consistent with the inability to attach acetophenone to saturated lipids. Other signals, for example *m*/*z* 770.527, are assigned to Norrish type I side products.

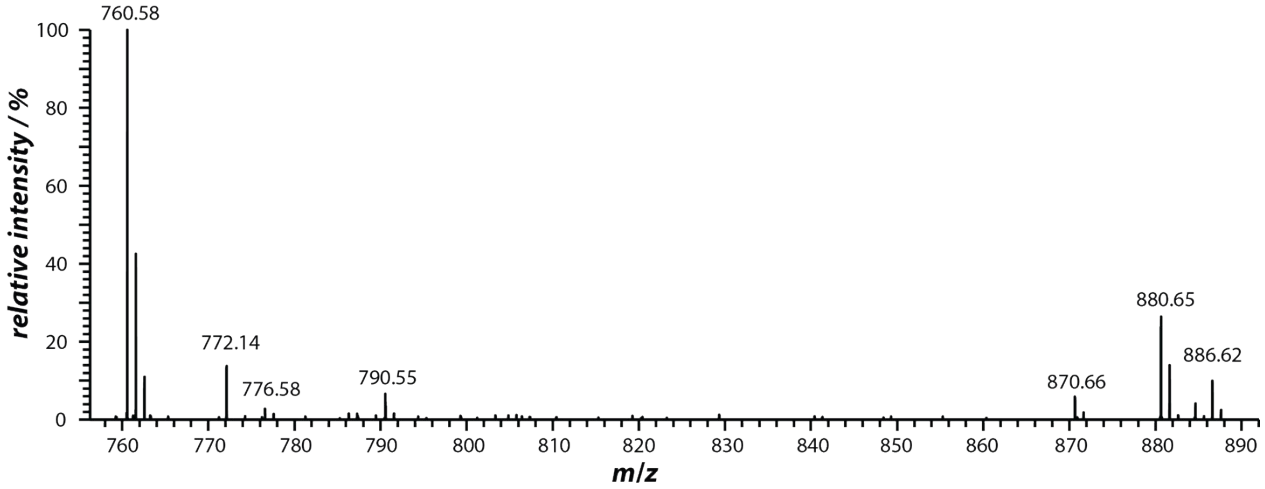

Figure S6. Positive nanoESI mass spectrum of protonated PC 16:0/18:1 (*m*/*z* 760.58) after 5 min UV irradiation. A 240 – 395 nm bandpass filter was used. Compared to **Figure 1b** several Norrish type I products are supressed because the 185 nm band of

the mercury lamp is blocked by the bandpass filter, whereas the PB reaction product is still observed (*m/z* 880.65).

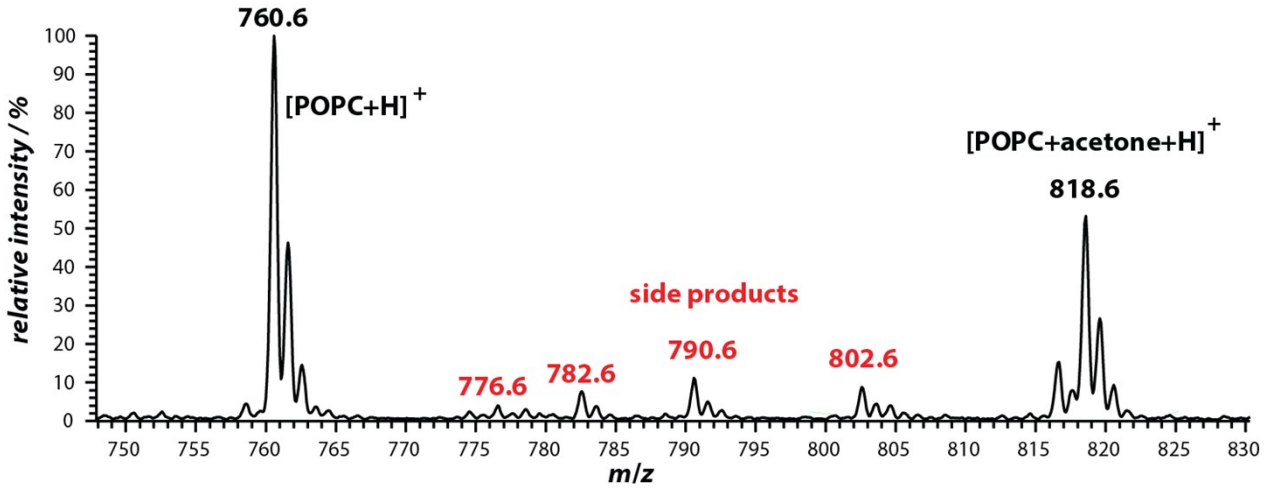

Figure S7. LTQ mass spectrum of POPC sprayed from an acidic acetone/water 50/50 solution irradiated for 60 s with 254 nm light. Protonated POPC, the protonated PB reaction product of POPC and some side products (red) are labeled with the corresponding *m*/*z*-values.

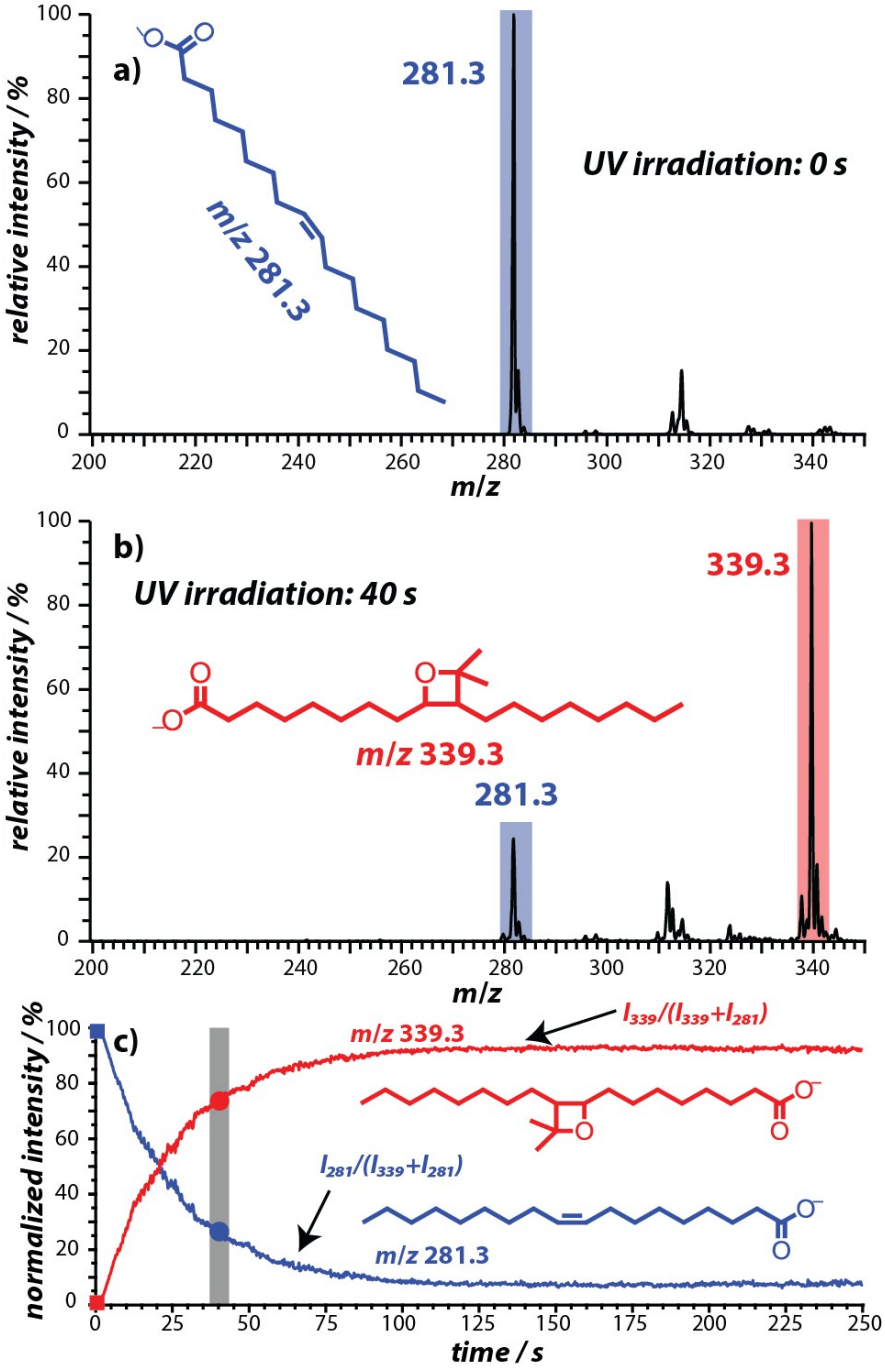

Figure S8. Negative ion mode nanoESI LTQ mass spectra of oleic acid sprayed from acetone/water 50/50 with 1% NH_4OH after a) 0 s and b) 40 s of irradiating a nanoESI emitter with 254 nm light. The [oleic acid-H]$^-$ and [oleic acid+acetone-H]$^-$ signals are

highlighted in blue and red, respectively. c) Reaction kinetics of the PB reactions between oleic acid and acetone as monitored by the corresponding protonated normalized ion signal intensities ($I_{281}/(I_{281+}\ I_{339})$ and $I_{339}/(I_{281+}\ I_{339})$). The squares and dots in c) indicate the data points that correspond to the mass spectra shown in b) and c), respectively. Possible structures of the ions of interest are included.

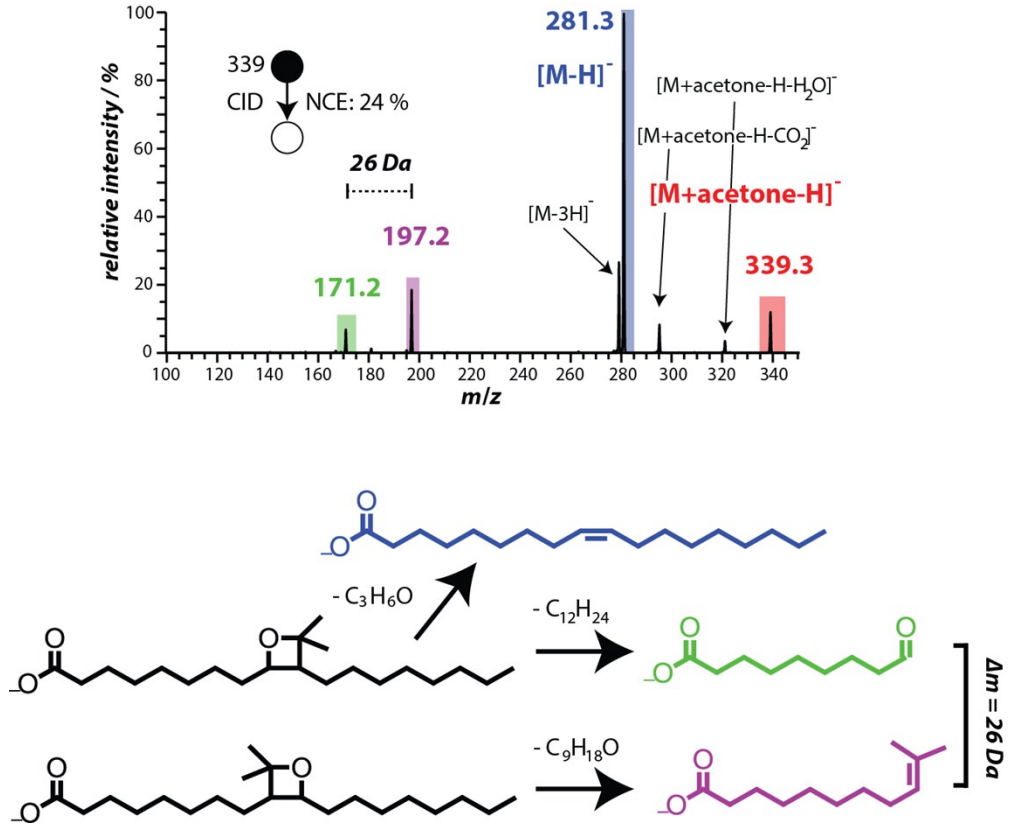

Figure S9. (upper) Negative ion mode CID tandem LTQ mass spectrum at NCE 24 of *m*/*z* 339.3. Signals are assigned to the PB reaction product of oleic acid and acetone (red), retro PB reaction to give deprotonated oleic acid (blue) and two double bond position specific ions (green and purple) with a mass difference of 26 Da.[3] Side products are shown in black. (lower) Fragmentation pathways of m/z 339.3 upon CID activation. Possible structures of fragment ions. Colour coded fragment ions correspond to the ion signals with the same colouring in the tandem mass spectrum.

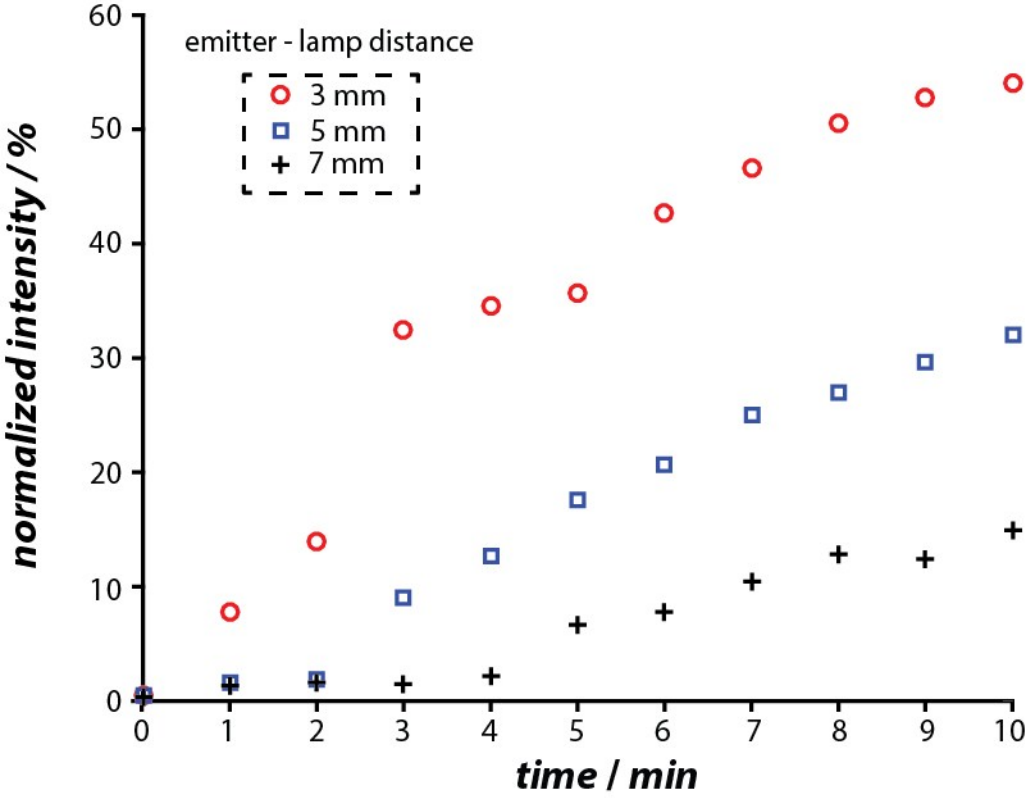

Figure S10. Maximum ion signal intensity ($[I_{339}/(I_{281+}\ I_{339})]_{max}$) of the oleic acid-acetone PB reaction product as a function of irradiation time (with 254 nm light) and emitter/Hg-lamp distance. Experiments were performed in negative ion mode using an acetone/water 50/50 solution with 1% NH_4OH, 10^{-5} M oleic acid concentration and a nanoESI emitter with ~5 µm inner diameter (larger diameter chosen to avoid saturation of the product ion signal). Emitters were irradiated for the indicated time with 254 nm light, irradiation was stopped, nanoESI spray was started by applying about -2 kV between MS inlet and nanoESI emitter and 20 mass spectra were averaged for every data point.

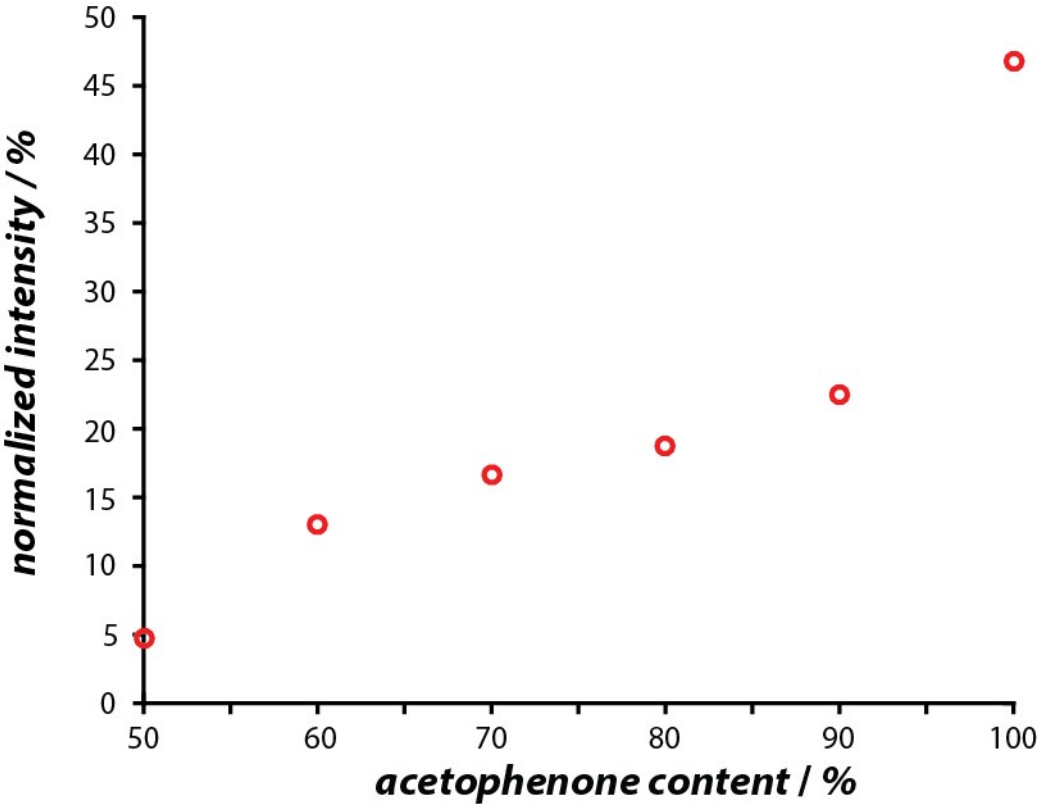

Figure S11. Maximum ion signal intensity ($[I_{880}/(I_{760+}\ I_{880})]_{max}$) of the POPC-acetophenone PB reaction product as a function of solvent composition (red circles). Experiments were performed in positive ion mode using acetophenone/ethanol solutions with 1% formic acid. The ratio between acetophenone and ethanol was varied between 50 – 100 % acetophenone. A 10^{-5} M POPC concentration and nanoESI emitters with ~5 µm inner diameter were used (larger diameter chosen to avoid saturation of the product ion signal). Emitters were irradiated for 5 min with 254 nm light, irradiation was stopped, nanoESI spray was started by applying about +2 kV between MS inlet and nanoESI emitter and 20 mass spectra were averaged for every data point.

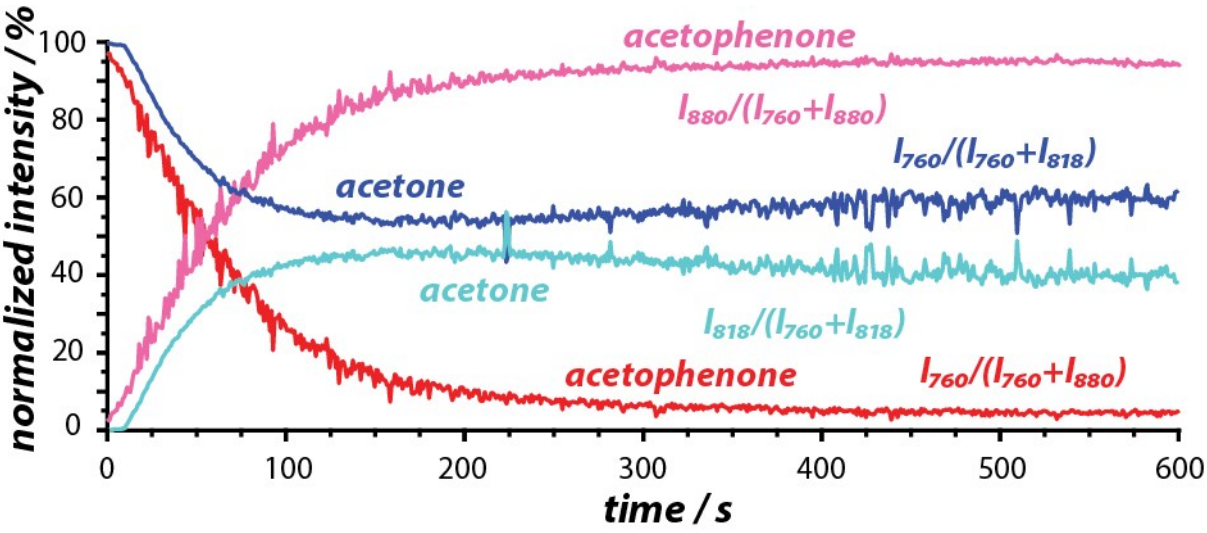

Figure S12. Comparison of the PB reaction kinetics of POPC with acetophenone (red/pink) and acetone (turquois/blue), respectively. One nanoESI emitter was filled with 10^{-5} M POPC in acetophenone + 1% formic acid and one emitter was containing 10^{-5} M POPC in 50 % water/50 % acetone with 1% formic acid, respectively. The ion source geometry was identical in both experiments and the lamp was allowed to cool prior to every experiment for at least 1 h. Protonated POPC (*m*/*z* 760) and the PB reaction products with acetophenone (*m*/*z* 880) and acetone (*m*/*z* 818) are monitored relative to the sum of the corresponding starting material and reaction product. The time scale of the acetone (blue/cyan) data is offset by + 10 s along x-axis in order to avoid overlap with the acetophenone data (red/pink).

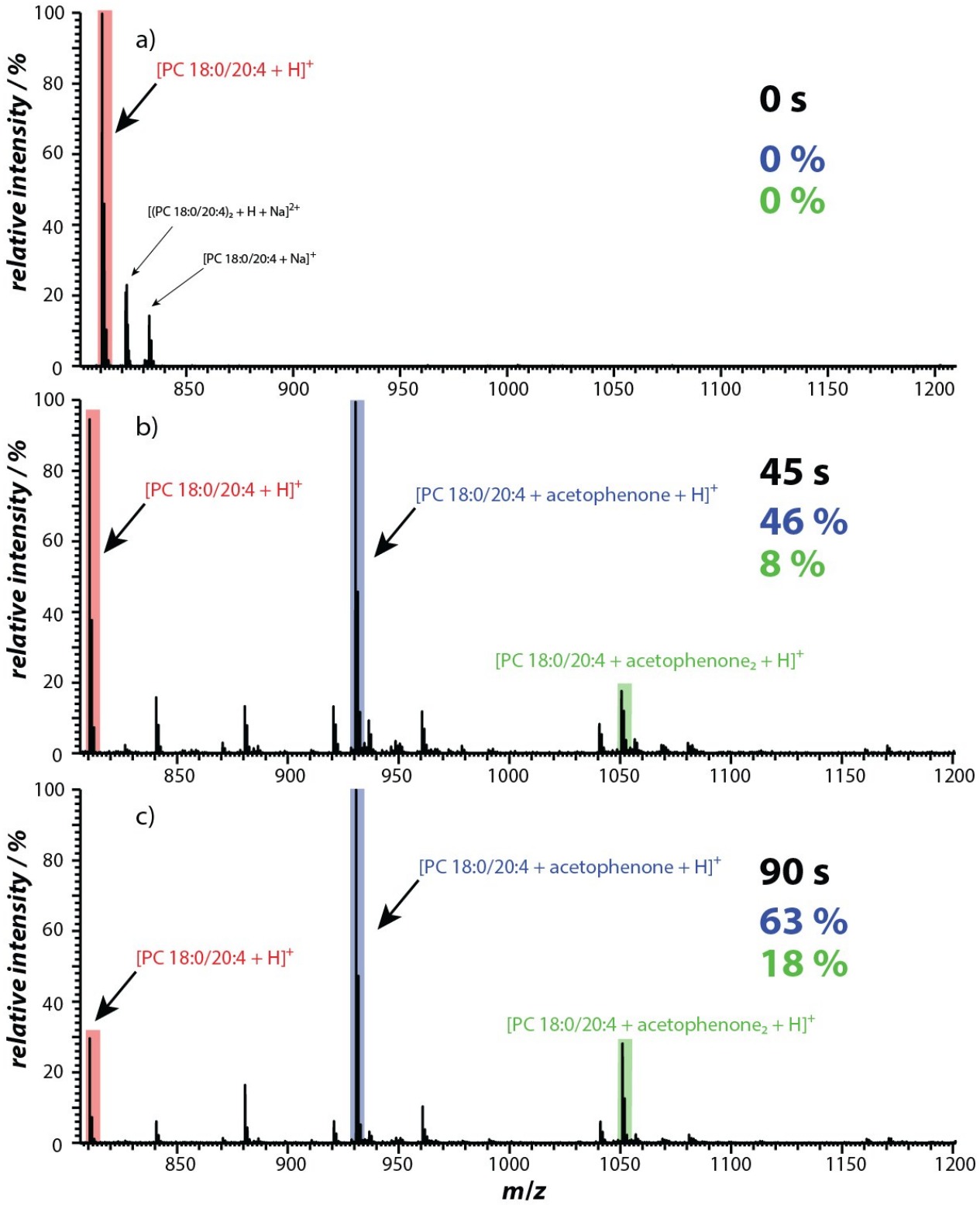

Figure S13. Positive ion mode mass spectra of 10^{-5} M PC 18:0/20:4 sprayed from acetophenone with 1% formic acid after a) 0 s, b) 45 s and b) 90 s of irradiating a

nanoESI emitter with 254 nm light. The $[PC\ 18:0/20:4+H]^+$, $[PC\ 18:0/20:4+acetophenone+H]^+$ and $[PC\ 18:0/20:4+(acetophenone)_2+H]^+$ signals are highlighted in red, blue and green, respectively. In a) some additional signals are assigned and the relative ion abundances, i.e. ion abundance of PB reaction product/(ion abundance of PB product + ion abundance of precursor) x 100 %, of $[PC\ 18:0/20:4+acetophenone+H]^+$ and $18:0/20:4+(acetophenone)_2+H]^+$ are included in blue and green, respectively.

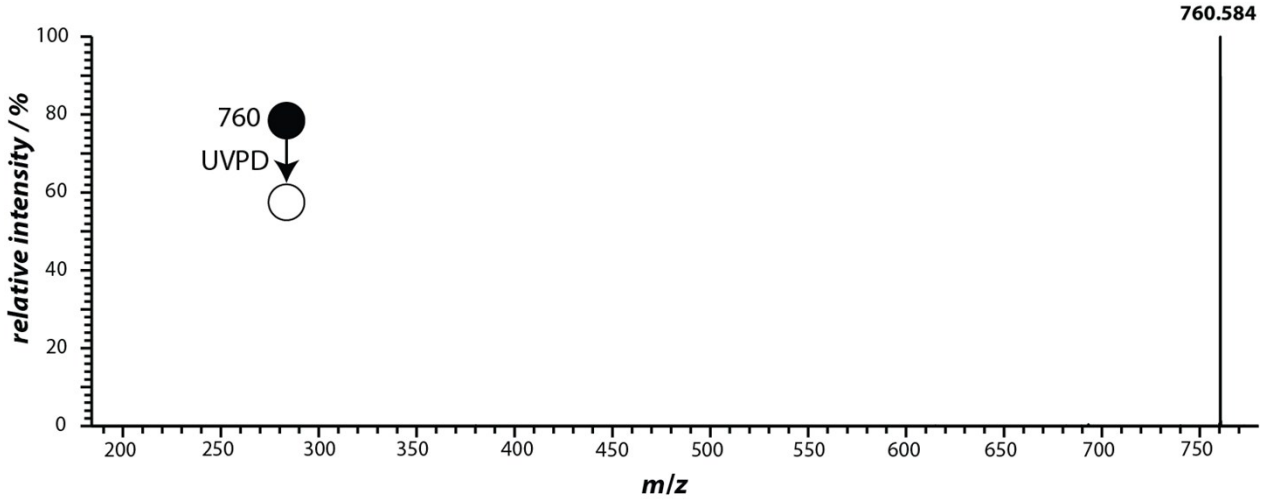

Figure S14. Identical to **Figure 2c** but showing the *m*/*z*-range 180-780.

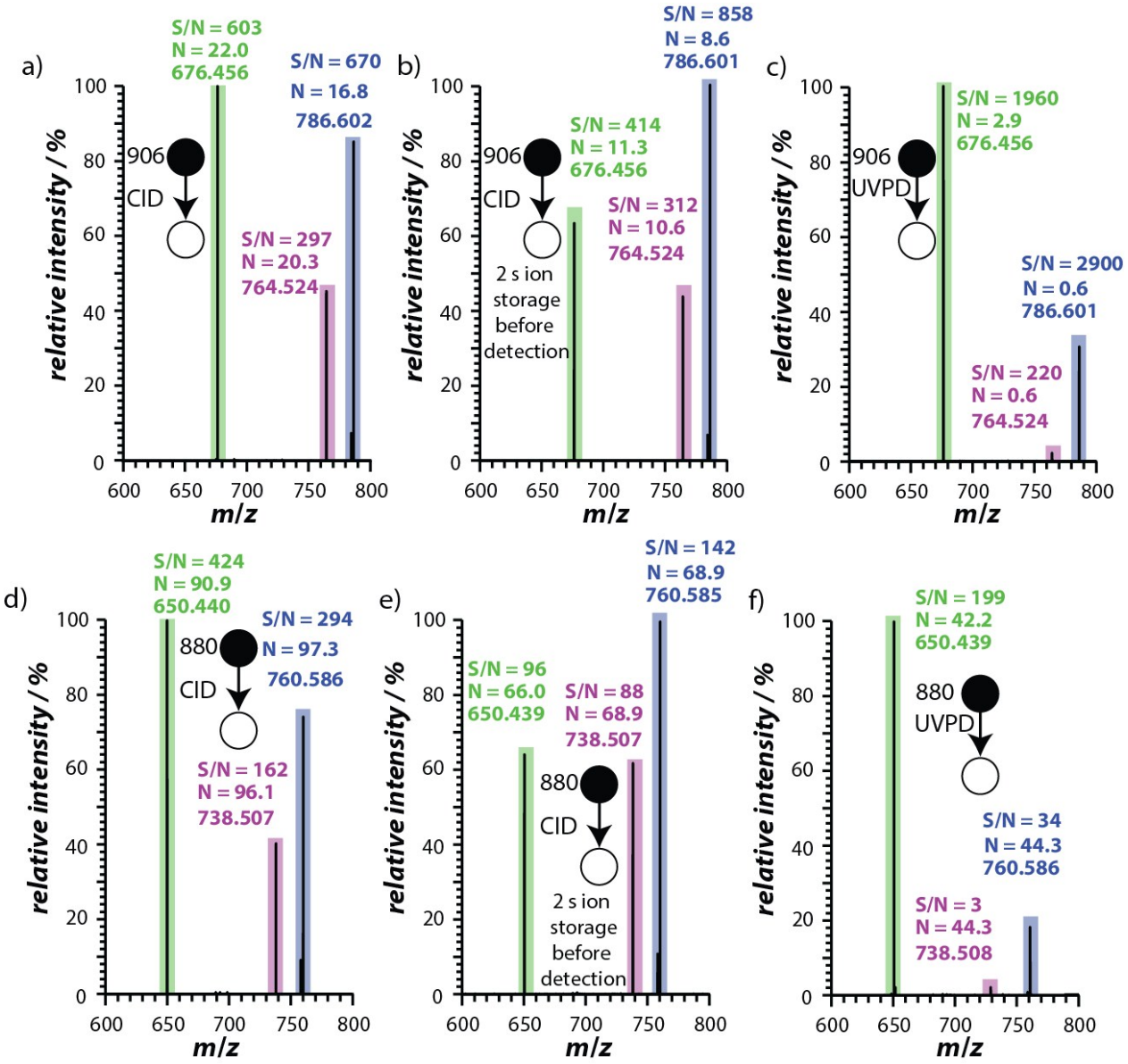

Figure S15. Comparison of S/N values between CID and UVPD results of acetophenone PB reaction products of protonated DOPC (a,b,c) and POPC (d,e,f). Acetophenone/DOPC (10^{-5} M) or acetophenone/POPC (10^{-5} M) with 1 % formic acid was irradiated for 100 s with UV light and the nanoESI spray was initiated. Using the same tip, ion source settings, instrument settings and number of averaged scans (50 scans) for all experiments, $[DOPC+acetophenone+H]^+$ was fragmented using a) CID (NCE 14), b) fragmented using CID (NCE 14) storing all ions for 2 s in the FT-ICR MS

before detection (thereby emulating the ion storage time used for UVPD experiments with 40 pulses) and c) performing UVPD (266 nm) measurements using 40 pulses and 0.6 mJ/pulse. Using the same tip, ion source settings, instrument settings and number of averaged scans (50 scans) for all experiments, $[POPC+acetophenone+H]^+$ was fragmented using a) CID (NCE 14), b) fragmented using CID (NCE 14) storing all ions for 2 s in the FT-ICR MS before detection (thereby emulating the ion storage time used for UVPD experiments with 40 pulses) and c) performing UVPD (266 nm) measurements using 40 pulses and 0.6 mJ/pulse. The noise levels (N), S/N values and experimental *m*/*z* values are included.

Dependence of S_{all} and *PY* on NCE levels in CID MS experiments

In order to study the effect of different CID and UVPD parameters on S_{all} and *PY*, protonated and acetophenone modified POPC and DOPC were investigated. For ion trap CID experiments the NCE setting were varied between 0 – 15 in a 0.5 step raster. Whereas *PY* of $[POPC+acetophenone+H]^+$ and $[DOPC+acetophenone+H]^+$ increases from 0 to 98 % (23 – 98 % for NCE 13 – 15) and from 0 to 96 % (50 – 96 % for NCE 13 – 15), respectively, S_{all} stays constant for $[POPC+acetophenone+H]^+$ and $[DOPC+acetophenone+H]^+$ within ±3% for NCE 13 – 15.

MS^3 experiments and energy per pulse dependence of PB-UVPD

In order to investigate possible fragmentations due to subsequent UV photon absorptions of retro-PB fragment ions during UVPD, MS^3 experiments were performed

and results are shown in **Figure S16**. $[POPC+acetophenone+H]^+$ was first fragmented using CID followed by 266 nm UVPD of *m*/*z* 738.508 (phenyl retro-PB ion) and *m*/*z* 650.440 (aldehyde retro-PB ion). The signal at *m*/*z* 760.585 observed in CID and UVPD experiments (**Figure 2**) does not fragment upon UVPD. Whereas UVPD of the aldehyde retro-PB ion (**Figure S16b**) results only in low abundance of PC headgroup loss (*m*/*z* 184.073), the corresponding UVPD of the phenyl retro-PB ion (**Figure S16a**) yields *m*/*z* 184.073 in high abundance. This indicates that the absence of the phenyl retro-PB ion type in PB-UVPD mass spectra is most likely due to UVPD of this ion type in the FT-ICR MS. This is also consistent with the high abundance of *m*/*z* 184.073 in **Figure S21** using 1.5 mJ/pulse. Head group loss could in part explain the PC ion head group loss, whereas the effect of internal vibrational energy redistribution is not well understood.

Additionally, $[POPC+acetophenone+H]^+$ and $[DOPC+acetophenone+H]^+$ were studied by UVPD as a function of laser energy per pulse with a fixed number of laser pulses (40 pulses) and results are shown in **Figure S17** and **Figure S18**. With increasing energy per pulse *PY* increases monotonically from 0 to up to 30 % (0 – 1 mJ/pulse) for $[POPC+acetophenone+H]^+$ and $[DOPC+acetophenone+H]^+$. For low laser energies per pulse S_{all} is 50 % (**Figure S17a**) and 59 % (**Figure S17b**), whereas S_{all} values increase with increasing laser energy per pulse and saturate at maximum values of 75 % (**Figure S17a**) and 73 % (**Figure S17b**) for $[POPC+acetophenone+H]^+$ and $[DOPC+acetophenone+H]^+$, respectively. The increase of S_{all} is predominantly determined by the increase of the retro-PB aldehyde ion abundance with respect to the neutral acetophenone loss (**Figure S18**), whereas other fragment ion channels such as retro-PB phenyl ion formation or neutral water loss vary only by ±3 % in relative abundance as a function of laser energy per pulse. These results indicate that most

likely a multi photon process such as photoisomerization followed by UVPD or sequential UV photon absorption followed by UVPD are responsible for the S_{all} increase in PB-UVPD experiments.

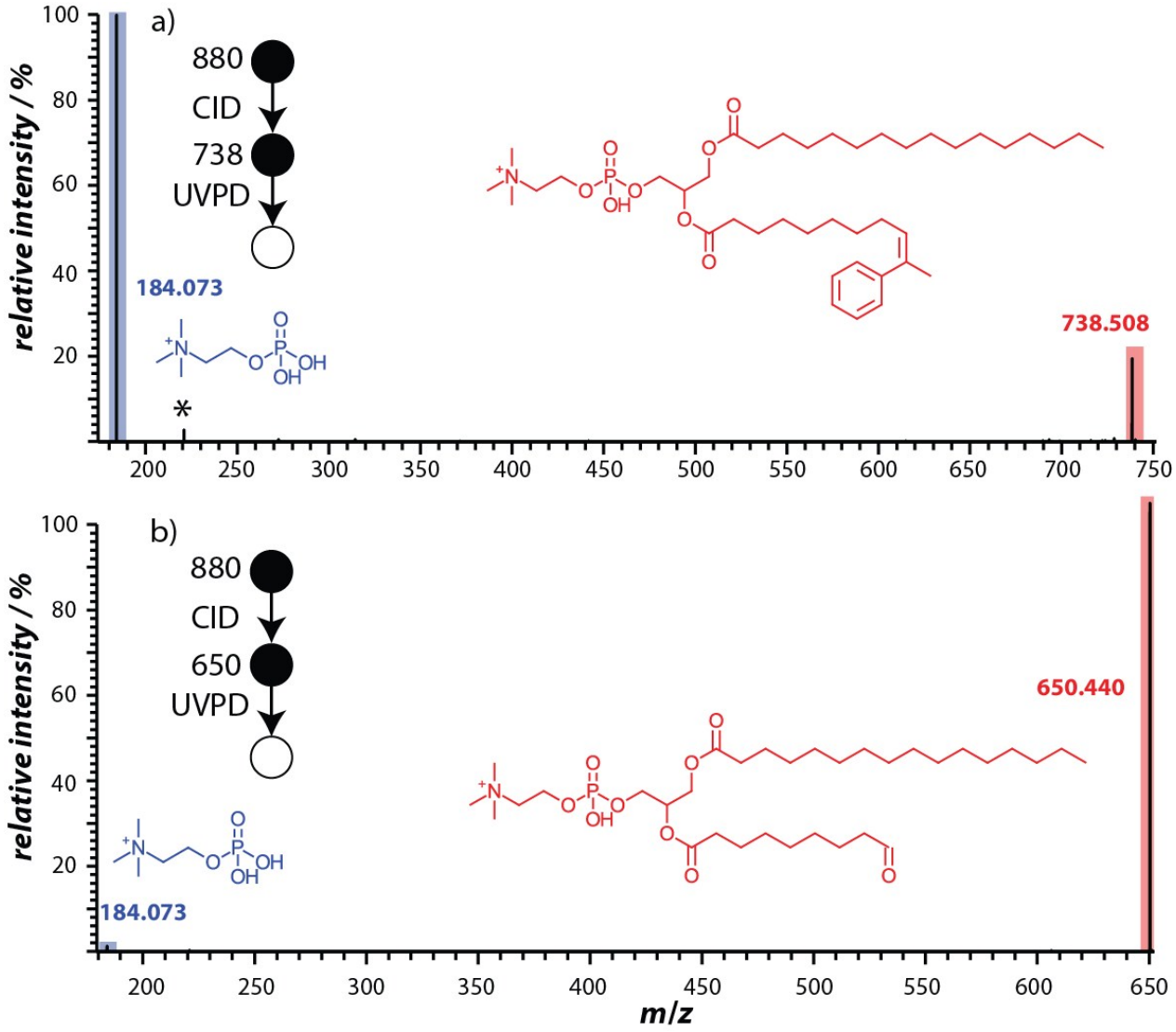

Figure S16. MS^3 (CID followed by 266 nm UVPD) experiments for $[POPC+acetophenone+H]^+$. First, $[POPC+acetophenone+H]^+$ was selected and fragmented using CID (NCE 14). Subsequently, 266 nm UVPD (0.6 mJ/pulse and 40 pulses) of retro-PB product ions at a) *m*/*z* 738.508 and b) *m*/*z* 650.440 were performed.

Precursor ion signals are colored red and product ion signals are highlighted in blue. Possible structures for ions are included. (*) Electronic noise.

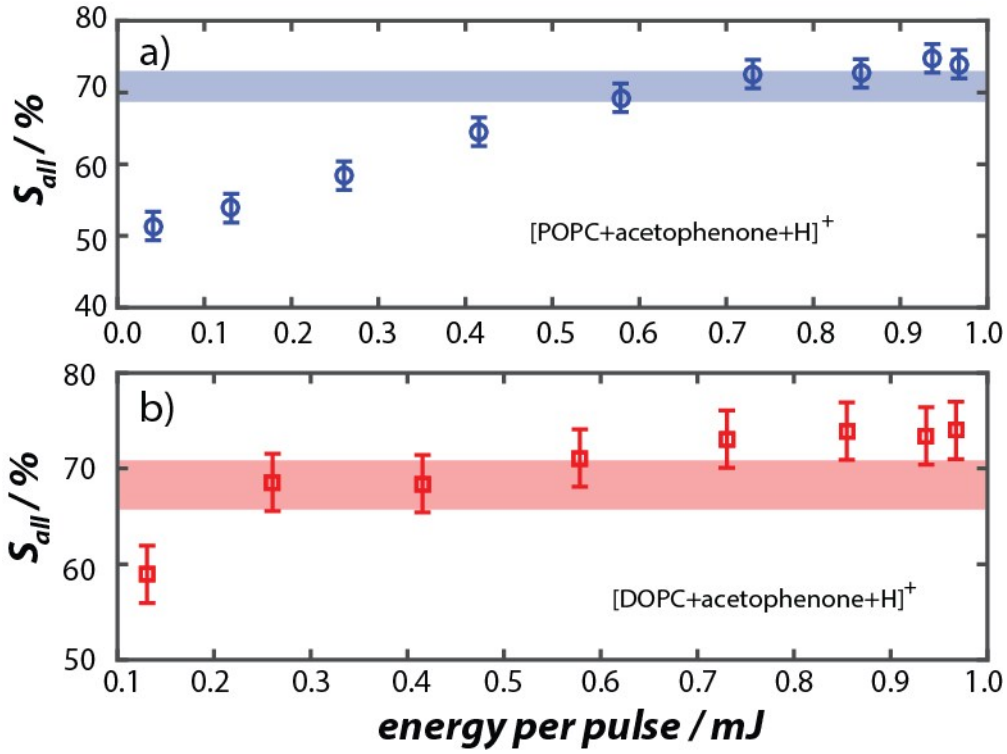

Figure S17. S_{all} of PB-UVPD experiments using 40 laser pulses as a function of laser energy per pulse for a) [POPC+acetophenone+H]$^+$ and b) [DOPC+acetophenone+H]$^+$. The colored blue and red area indicates the values and corresponding errors reported in the main manuscript.

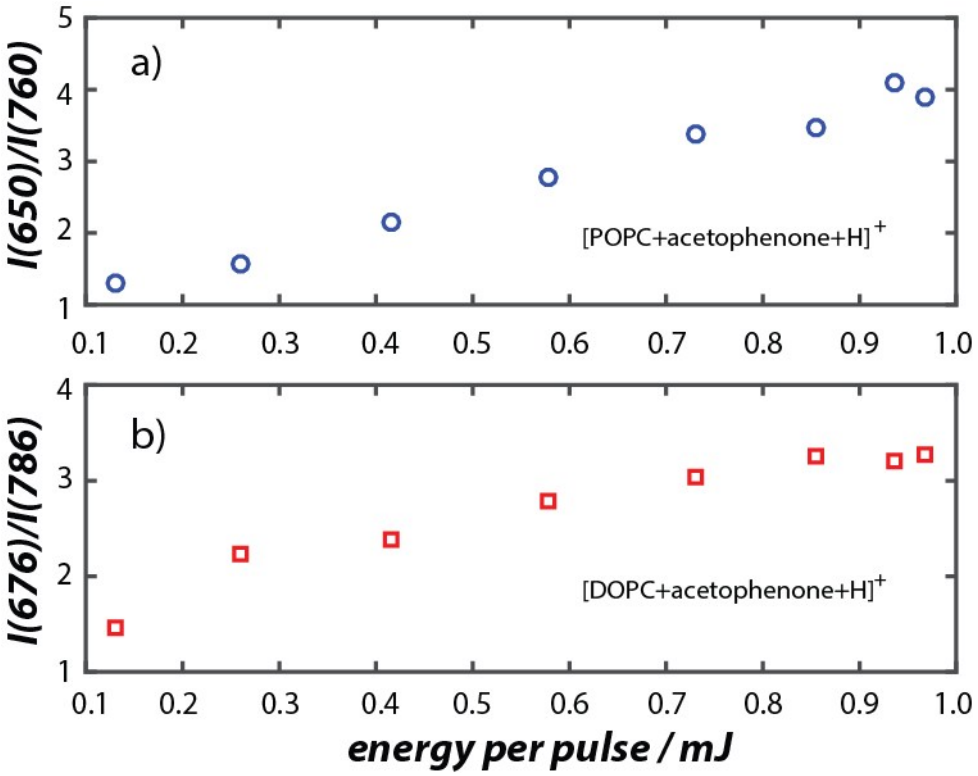

Figure S18. Retro-PB aldehyde fragment ion abundance relative to the ion abundance associated with the neutral loss of acetophenone as a function of energy per pulse in PB-UVPD experiments (40 pulses) for a) $[POPC+acetophenone+H]^+$ and b) $[DOPC+acetophenone+H]^+$.

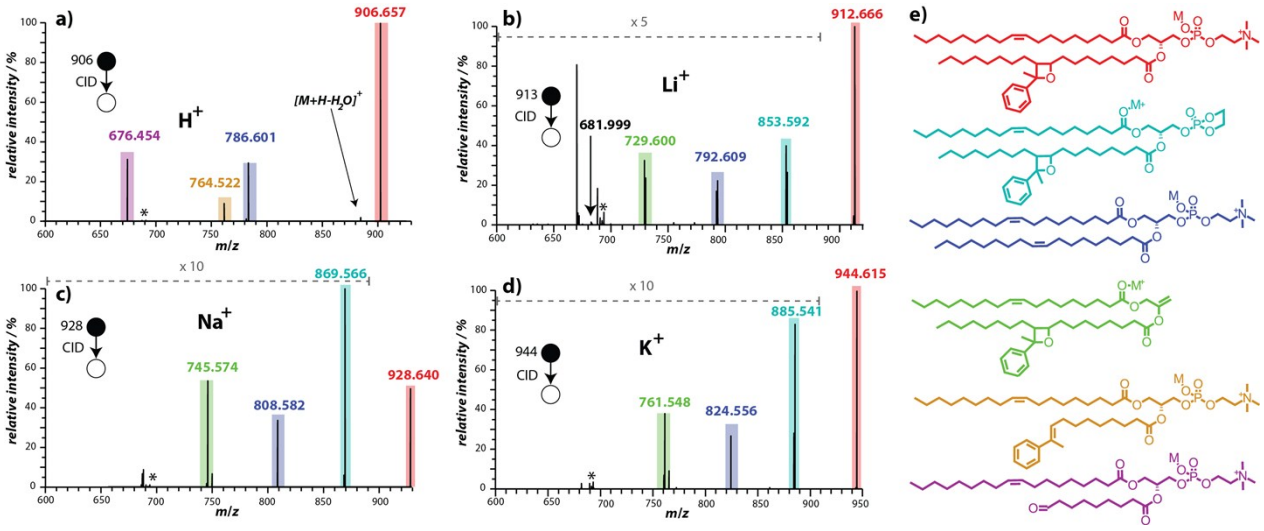

Figure S19. CID tandem mass spectra (NCE 25) of (a) $[DOPC+acetophenone+H]^+$, (b) $[DOPC+acetophenone+Li]^+$, (c) $[DOPC+acetophenone+Na]^+$ and (d) $[DOPC+acetophenone+K]^+$. Experimental *m*/*z*-values are included, assigned fragment ion signals are colour coded and possible fragment ion structures with $M^+ = H^+$, Li^+, Na^+, K^+ are shown in (e). (*) Electronic noise.

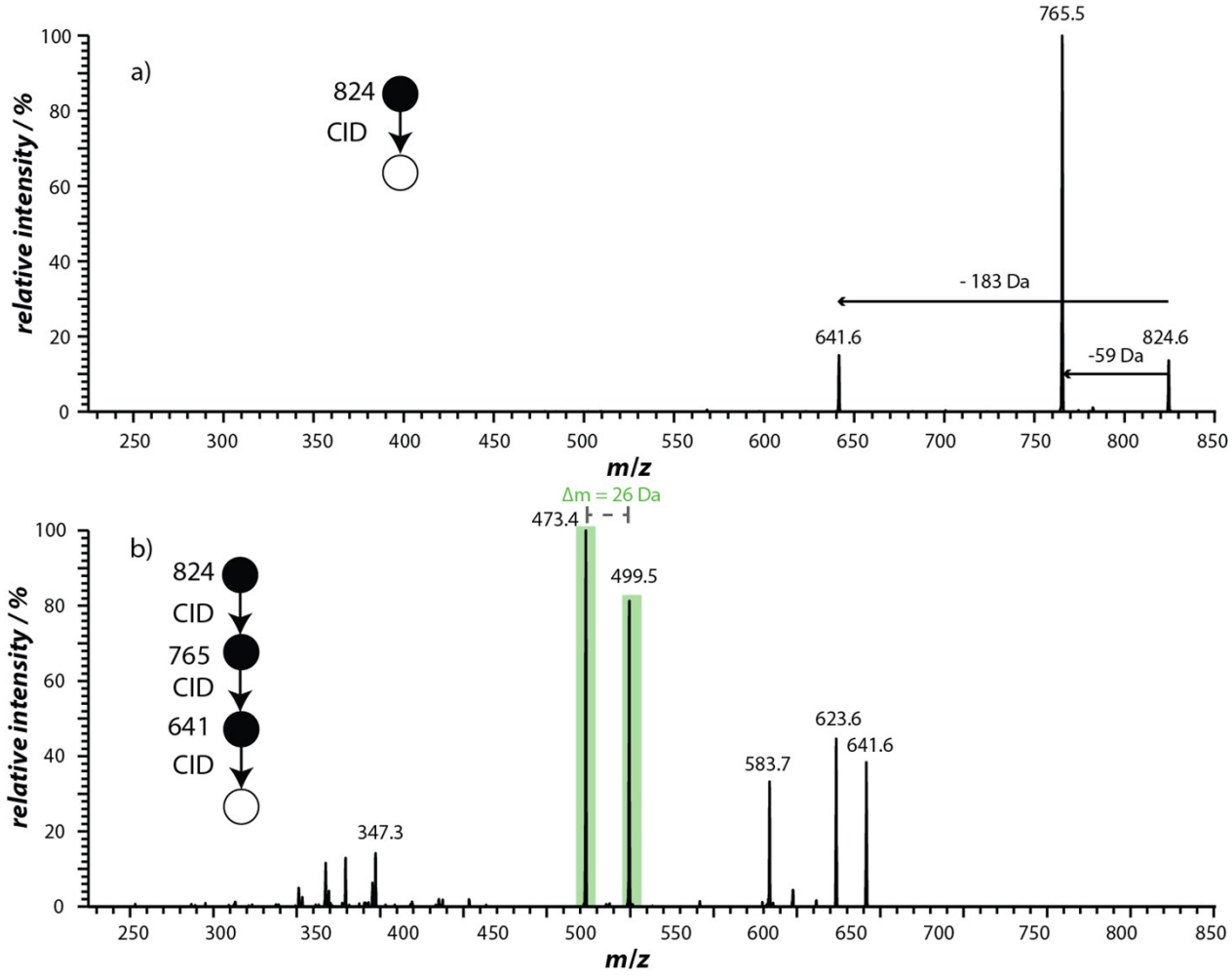

Figure S20. LTQ tandem mass spectra of $[POPC+acetone+Li]^+$. (a) MS^2 of *m*/*z* 824.6 results in the loss of trimethylamine (-59 Da) and the phosphocholine head group (-183 Da). (b) MS^4 (*m*/*z* 824.6 to *m*/*z* 765.5 to *m*/*z* 641.6) gives the two double bond-specific fragment ions *m*/*z* 473.4 and *m*/*z* 499.5.

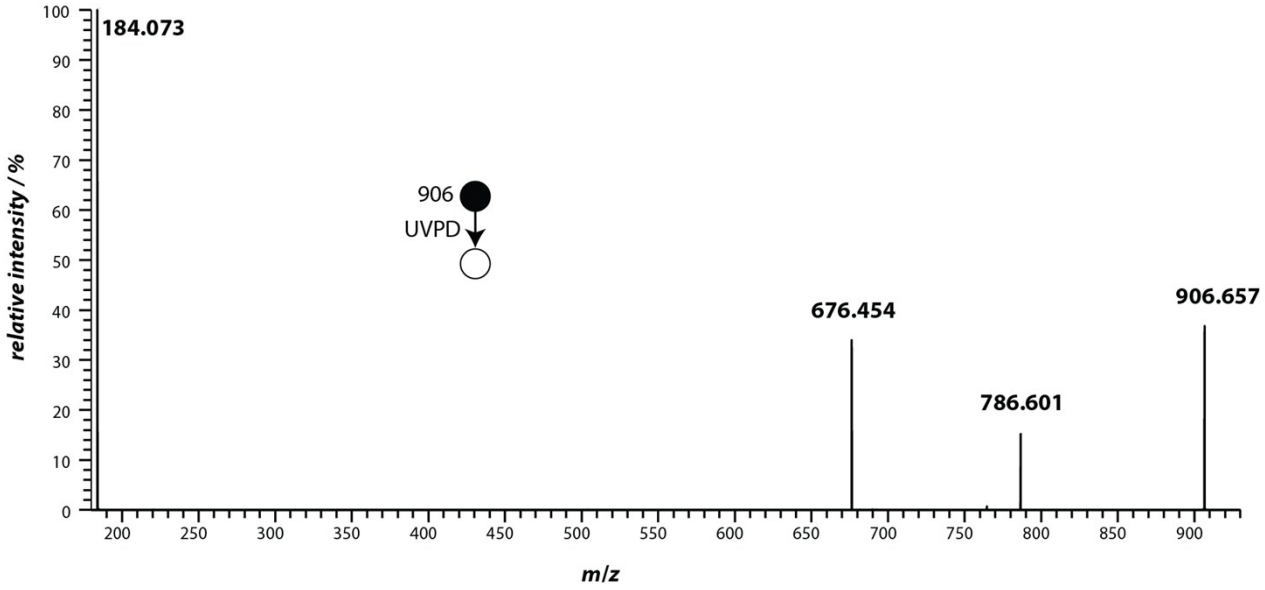

Figure S21. UVPD tandem mass spectrum of $[DOPC+acetophenone+H]^+$ using 1.5 mJ/pulse and 40 laser pulses. Experimental *m*/*z*-values are included.

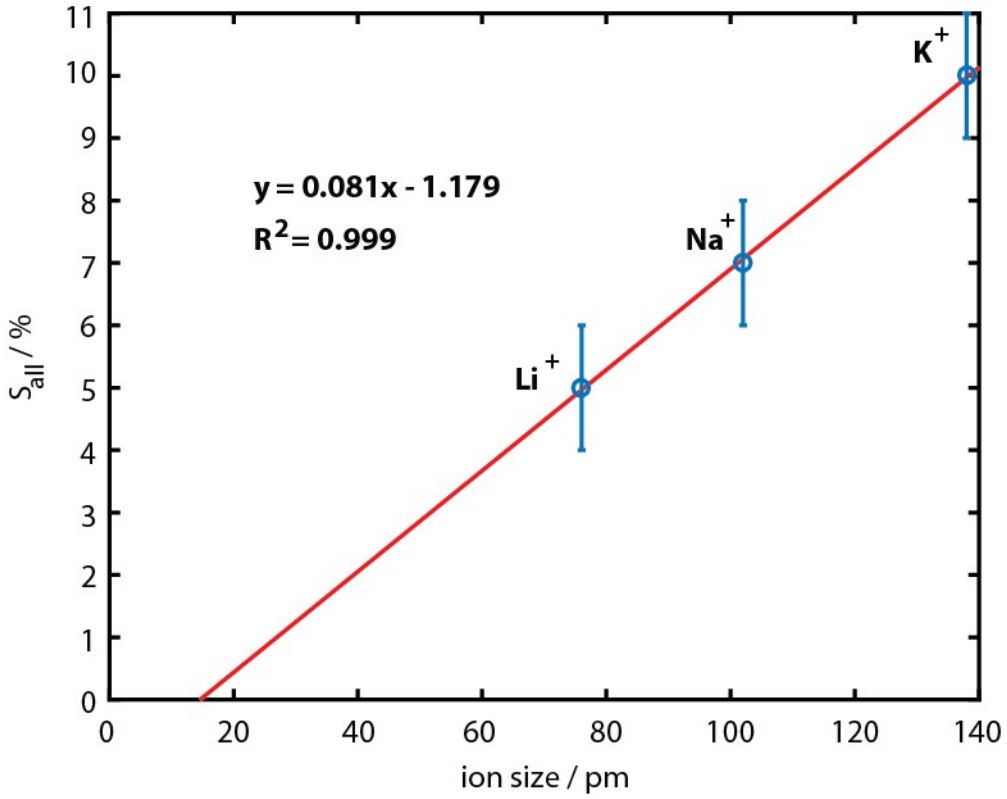

Figure S22. S_{all} as a function of size of the DOPC+acetophenone attached ion. Experimental data and error shown in blue and linear fit shown in red. Ionic sizes were taken from ref.[4].

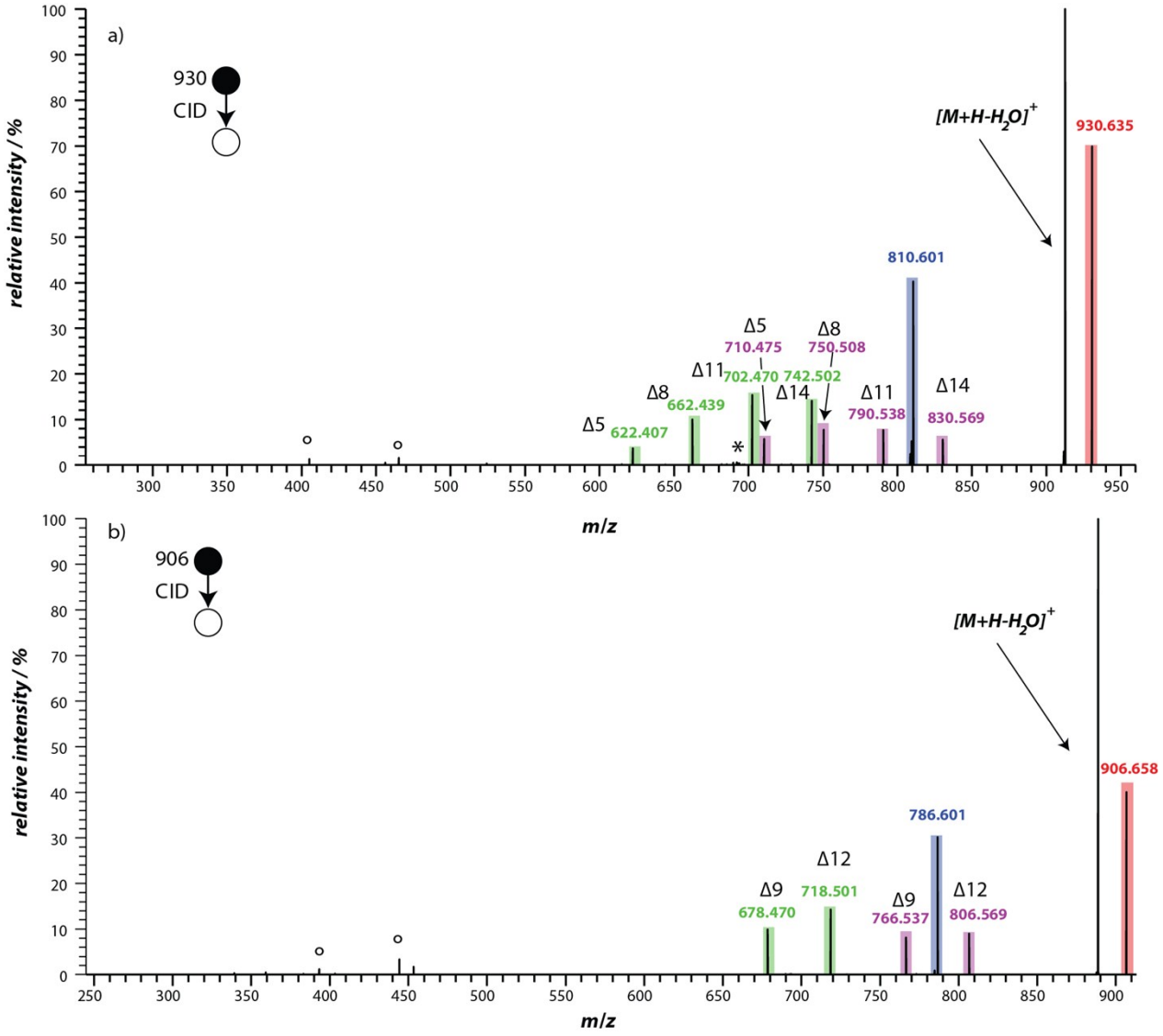

Figure S23. CID tandem mass spectra (NCE 22) of protonated and acetophenone modified (a) PC 18:0/20:4(Δ5, Δ8, Δ11, Δ14) and (b) PC 18:0/18:2(Δ9, Δ12) lipids. Experimental *m*/*z*-values are included and double bond position specific fragments are labelled with the corresponding double bond position. (°) Second harmonic signals; (*) electronic noise.

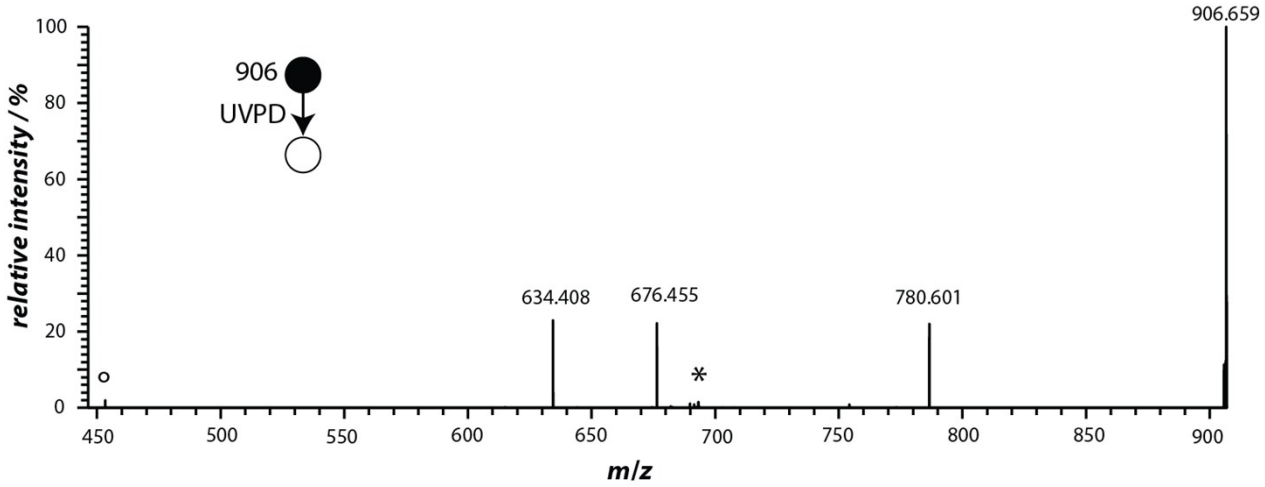

Figure S24. UVPD tandem mass spectrum (1 mJ/pulse, 40 pulses) of *m*/*z* 906.659 from an acidic solution containing a 1:1 mixture of PC 18:1(Δ9)/18:1(Δ9) : PC 18:1(Δ6)/18:1(Δ6). (°) Second harmonic signals; (*) electronic noise.

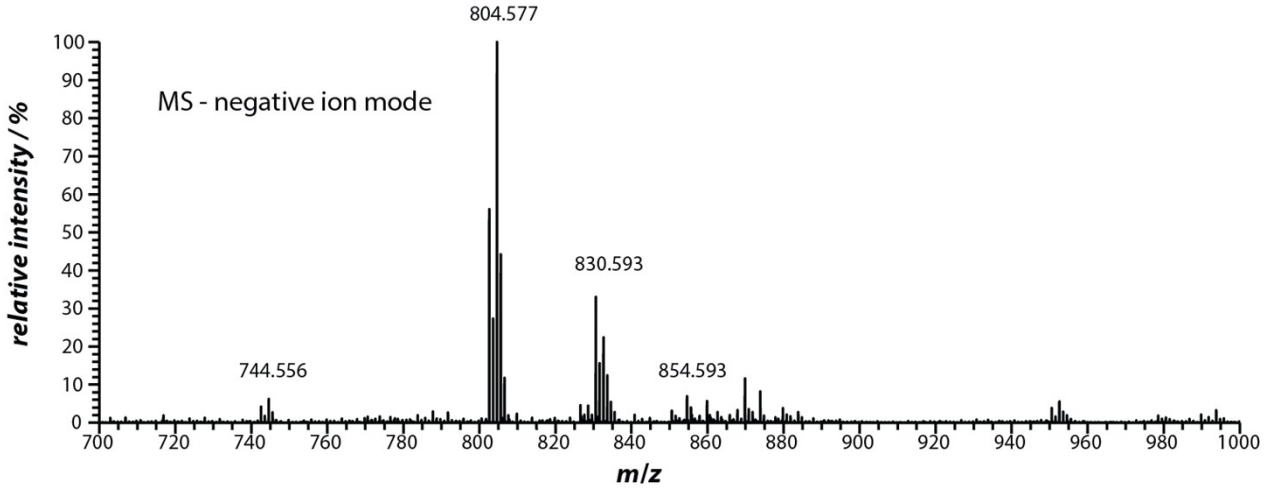

Figure S25. Negative ion mode mass spectrum of polar lipid egg yolk extract sprayed from methanol solution containing 100 µg/mL lipid extract and 30 mM ammonium formate. Phosphatidylcholines (PCs) are detected as $[PC + formate]^-$ ions. Some signals are labelled with the corresponding experimental *m*/*z*-values.

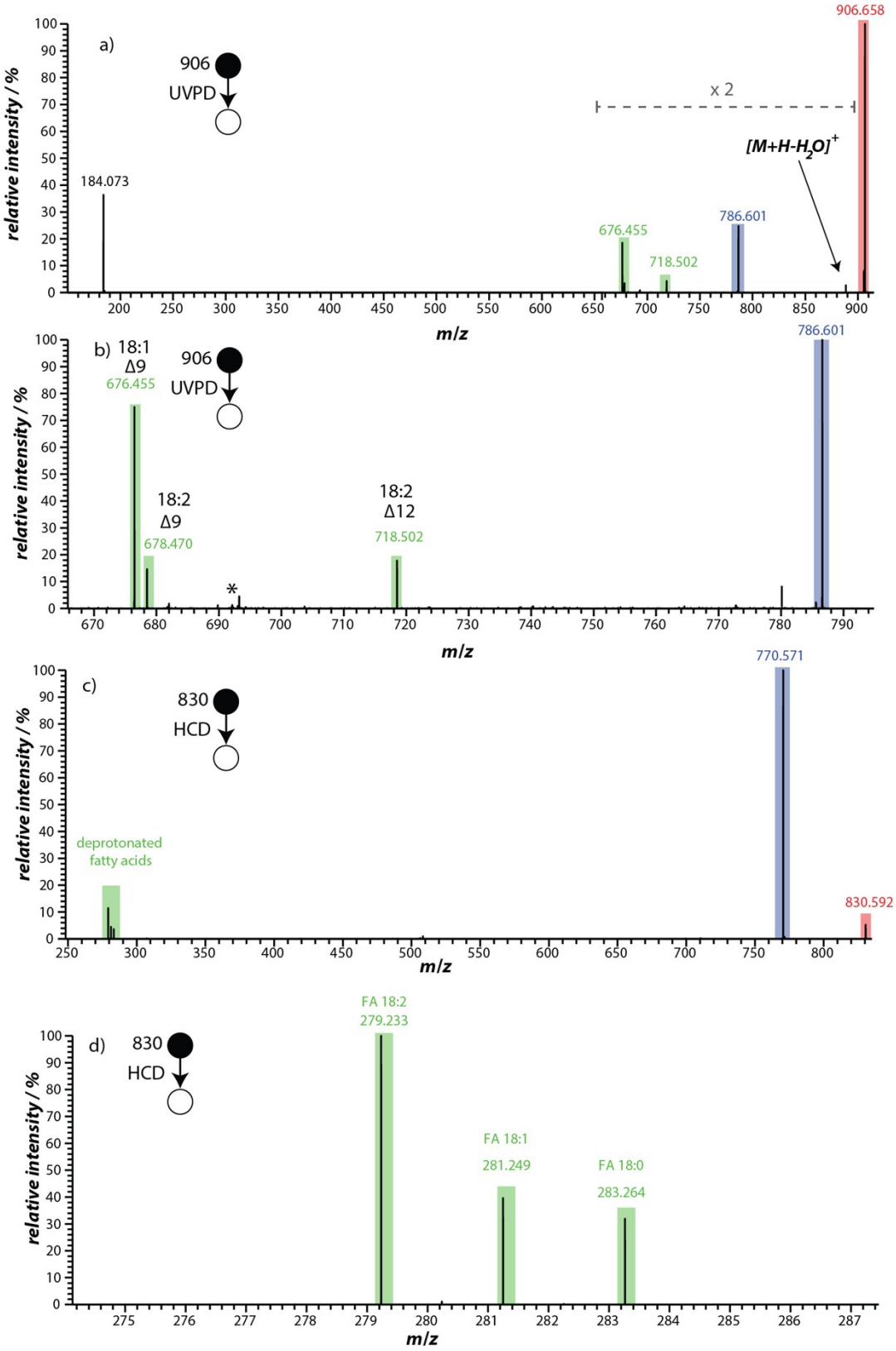
a)
906
UVPD
x 2
[M+H-H2O]+
906.658
184.073
676.455
718.502
786.601
relative intensity / %
m/z
b) 18:1
Δ9
676.455
906
UVPD
18:2
Δ9
678.470
18:2
Δ12
718.502
786.601
*
relative intensity / %
m/z
c)
830
HCD
deprotonated
fatty acids
770.571
830.592
relative intensity / %
m/z
d)
830
HCD
FA 18:2
279.233
FA 18:1
281.249
FA 18:0
283.264
relative intensity / %
m/z

Figure S26. Example for the double bond position and fatty acid chain identification of PCs from polar lipid egg yolk extract. (a) Positive ion mode UVPD tandem overview mass spectrum (40 pulses, 1 mJ/pulse) of *m*/*z* 906.658. (b) Expansion of *m*/*z* 668 – 795 of the spectrum shown in (a). Double bond position specific fragments are labelled. (c) Negative ion mode HCD tandem mass spectrum (NCE 25) of *m*/*z* 830.592. (d) Expansion of *m*/*z* 271-288 shown in (c). Colour coding: green – structure sensitive fragment ions; red – protonated molecular ion; blue – loss of neutral acetophenone or formic acid. (*) Electronic noise.

References

1 A. Herburger, C. van der Linde and M. K. Beyer, *Phys. Chem. Chem. Phys.*, 2017, **19**, 10786–10795.
2 B. B. Kirk, A. J. Trevitt, S. J. Blanksby, Y. Tao, B. N. Moore and R. R. Julian, *J. Phys. Chem. A*, 2013, **117**, 1228–1232.
3 X. Ma and Y. Xia, *Angew. Chem. Int. Ed.*, 2014, **53**, 2592–2596.
4 Ulrich Müller, *Anorganische Strukturchemie*, Teubner Verlag, Wiesbaden, 5. Auflage, 2006.